Theoretical and Mathematical Physics, **183**(3): 846–859 (2015)

SUBDIFFUSION KINETICS OF NANOPRECIPITATE GROWTH AND DESTRUCTION IN SOLID SOLUTIONS

R. T. Sibatov* **and V. V. Svetukhin***

Based on fractional differential generalizations of the Ham and Aaron–Kotler precipitation models, we study the kinetics of subdiffusion-limited growth and dissolution of new-phase precipitates. We obtain the time dependence of the number of impurities and dimensions of new-phase precipitates. The solutions agree with the Monte Carlo simulation results.

Keywords: subdiffusion, nanoprecipitate, fractional derivative, supersaturated solid solution, Monte Carlo method

1. Introduction

As is known, diffusion models were successfully used to describe the decomposition of supersaturated solid solutions (precipitation) at the stage of new-phase precipitate growth [1]–[10]. They are based on the concept of normal impurity diffusion. But a series of experimental facts demonstrate anomalous diffusion (predominantly subdiffusion) of impurities and defects in various materials [11]–[15]. It is conventionally characterized using the law of expansion of the diffusion packet $\Delta(t) \propto t^{\alpha/2}$.

Classical diffusion ($\alpha = 1$) is based on Gaussian statistics and the second Fick law, which lead to the dependence $\Delta(t) = \sqrt{\langle x^2(t)\rangle} \propto t^{1/2}$ [16]. The diffusion packet width increases with time more slowly (subdiffusion) in the case $0 < \alpha < 1$ and more rapidly (superdiffusion) in the case $\alpha > 1$ than in the normal case. Equations containing fractional derivatives form the mathematical basis of anomalous self-similarity diffusion [14], [17], [18].

Existing diffusion models of precipitation rather incompletely reflect the properties of transport phenomena occurring in actual materials, for which the presence of disorder leads to a significant change in the diffusion type [12], [13]. Using diffusion equations containing fractional derivatives allows considerably simplifying the consideration of complex phenomena, such as diffusion in inhomogeneous media and diffusion along grain boundaries and dislocations [14], [18].

Here, we study the subdiffusion-limited kinetics of the growth and decomposition of new-phase precipitates using fractional differential generalizations of classical models of precipitate growth and dissolution in solid solutions [2], [3], [7]. As a tool for describing anomalous diffusion in disordered media, we use the dispersive transport theory developed in [18]–[21].

We compare the analytic solutions with the results of a Monte Carlo simulation of the process.

*Laboratory of Diffusion Process Modeling, Ulyanovsk State University, Ulyanovsk, Russia, e-mail: ren_sib@bk.ru.

Translated from Teoreticheskaya i Matematicheskaya Fizika, Vol. 183, No. 3, pp. 460–476, June, 2015. Original article submitted December 3, 2014.

2. Random walks with impurity localization

To describe hereditary particle diffusion (diffusion with a delay related to localization times), an integro-differential equation of the form

$$\frac{\partial\rho(\mathbf{r},t)}{\partial t} = C\int_0^t d\tau\, Q(t-\tau)\nabla^2\rho(\mathbf{r},t) \tag{1}$$

is often used [14], [22], where $Q(t)$ is the memory kernel and ρ is the total particle concentration (localized and mobile). In this case, the Fick law $\mathbf{j}(\mathbf{r},t) = -D\nabla\rho(\mathbf{r},t)$ is inapplicable, and the generalized Fick law must be used [23]. Equation (1) can be obtained using the continuous-time random walk (CTRW) model [24]–[29]. It is assumed that particles change their positions by hopping at arbitrary times; the intervals between hops (*waiting times*) are independent equally distributed random variables τ.

The integral equation of the CTRW model for the distribution density of the walking-particle coordinate x at the instant t has the form [29]

$$\rho(\mathbf{r},t) = \Psi(t)\delta(\mathbf{r}) + \int\limits_0^t dt'\,\psi(t')\int d\mathbf{r}'\,w(\mathbf{r}')\rho(\mathbf{r}-\mathbf{r}',t-t'), \tag{2}$$

where $\psi(t)$ is the density of the residence time distribution for particles in the localized states, $\Psi(t) = \int_t^\infty d\tau\,\psi(\tau)$ is the additional distribution function, and $w(\mathbf{r})$ is the density of elementary displacement distribution. It is assumed that the particle is in the localized state at the coordinate origin at $t = 0$.

The Fourier–Laplace transformation of Eq. (2) leads to the algebraic relation from which the image of the function $\rho(\mathbf{r},t)$ (the Montroll–Weiss formula [30]) can be found,

$$\widetilde{\hat{\rho}}(\mathbf{k},s) = \frac{\widetilde{\Psi}(s)}{1-\hat{w}(\mathbf{k})\tilde{\psi}(s)}, \qquad \widetilde{\hat{\rho}}(\mathbf{k},s) = \int_0^t dt\int d\mathbf{r}\,e^{i\mathbf{k}\mathbf{r}-st}\rho(\mathbf{r},t), \tag{3}$$

where $\hat{w}(\mathbf{k})$ is the Fourier transform of the function $w(\mathbf{r})$ and $\widetilde{\Psi}(s)$ is the Laplace transform of $\Psi(t)$ related to the Laplace transform of the distribution density by the expressions

$$\widetilde{\Psi}(s) = \frac{1-\tilde{\psi}(s)}{s}, \qquad \tilde{\psi}(s) = 1 - s\widetilde{\Psi}(s). \tag{4}$$

Substituting the expansion of the characteristic function of the displacement distribution density with a zero mean and the finite dispersion $\hat{w}(\mathbf{k}) \sim 1 - C|\mathbf{k}|^2$ for small $|\mathbf{k}|$ and expression (4) in Montroll–Weiss equation (3) leads to an equation that can be written in the two equivalent forms

$$\left[s + C\frac{\tilde{\psi}(s)}{\widetilde{\Psi}(s)}|\mathbf{k}|^2\right]\tilde{\rho}(k,s) = 1, \tag{5}$$

$$\left[\frac{s\widetilde{\Psi}(s)}{\tilde{\psi}(s)} + C|\mathbf{k}|^2\right]\tilde{\rho}(k,s) = \frac{\widetilde{\Psi}(s)}{\tilde{\psi}(s)}. \tag{6}$$

The inverse Fourier–Laplace transformation of the first of them leads to hereditary diffusion equation (1), where the image of the memory kernel has the form $\widetilde{Q}(s) = \tilde{\psi}(s)/\widetilde{\Psi}(s)$. For Eq. (6), we can write

$$\frac{\partial}{\partial t}\int_0^t d\tau\,\rho(\mathbf{r},\tau)\Phi(t-\tau) - C\nabla^2\rho(\mathbf{r},t) = \delta(\mathbf{r})\Phi(t), \tag{7}$$

where $\Phi(t)$ is the original for the Laplace image $\widetilde{\Phi}(s) = \widetilde{\Psi}(s)/\tilde{\psi}(s)$.

It can be shown [17] that requiring the Green's function of Eq. (1) to be self-similar leads to the fractional differential diffusion equation

$$\frac{\partial \rho(\mathbf{r},t)}{\partial t} = C_\alpha \nabla^2 \, {}_0\mathsf{D}_t^{1-\alpha} \rho(\mathbf{r},t). \tag{8}$$

Here,

$${}_0\mathsf{D}_t^{\alpha} \rho(\mathbf{r},t) = \frac{1}{\Gamma(1-\alpha)} \frac{\partial}{\partial t} \int_0^t d\tau \, \frac{\rho(\mathbf{r},\tau)}{(t-\tau)^\alpha}$$

is the Riemann–Liouville fractional derivative [31]–[33]. The derivative order is determined by the dispersion parameter $0 < \alpha \leq 1$, which can be found from the experiment. The fundamental solutions of this equation were given in [17], [31]. Fractional differential equation (8) can be derived as an asymptotic form of Eq. (1) in the case of a power series distribution of localization times:

$$\Psi(t) = P\{\tau > t\} \propto t^{-\alpha}, \quad \alpha > 0, \quad t \to \infty. \tag{9}$$

Indeed, substituting the expressions for the Laplace transforms $\tilde{\psi}(s) = 1 - b_\alpha s^\alpha$ and $\widetilde{\Psi}(s) = b_\alpha s^{\alpha-1}$ in Eq. (5) in the asymptotic form as $s \to 0$ leads to the expression

$$[s + C_\alpha s^{1-\alpha} |\mathbf{k}|^2] \tilde{\rho}(k,s) = 1, \qquad C_\alpha = \frac{C}{b_\alpha}, \tag{10}$$

whose inverse Laplace transform gives Eq. (8) with the initial condition $\rho(\mathbf{r},t)|_{t=0} = \delta(\mathbf{r})$.

We note that it is convenient to represent the subdiffusion equation in form (8) in order to write the continuity equation

$$\frac{\partial \rho}{\partial t} + \operatorname{div} \mathbf{j} = 0, \tag{11}$$

where the particle current density is expressed in terms of the concentration using the generalized Fick law [23]

$$\mathbf{j} = -C \, {}_0\mathsf{D}_t^{1-\alpha} \nabla \rho(\mathbf{r},t). \tag{12}$$

We use Eqs. (8) and (12) to analyze the kinetics of subdiffusion growth and disssolution of new-phase particles.

Mechanisms for anomalous diffusion are various [12], [14], [18]. The fact that subdiffusion can be observed as a result of normal diffusion in an inhomogeneous medium seems noteworthy to us. Figure 1 shows the results of simulating the walk of a particle (impurity atom or vacancy) on a planar realization of the spinodal decomposition of a two-component solution in the case of equal fractions of the components. The realization was obtained using the Monte Carlo method in the framework of the Cahn–Hilliard approach [34]–[36]. In the calculation, we assumed that the cross section for isotropic scattering of the walking particle depends on the solution composition in accordance with the formula $\sigma = \sigma_0 e^{-c/c_0}$, where $0 \leq c \leq 1$ is the fraction of one of the components. The results in Fig. 1 are given for the case $c_0 = 0.3$. The region of subdiffusion behavior is observed in the time dependence of the average squared particle displacement. The diffusion becomes normal at large times. Such behavior can be explained by the presence of regions with a low diffusion coefficient ($c \approx 1$; see Fig. 1b), which serve as a Brownian trap for walking particles. The times of localization in these regions are distributed in accordance with a truncated power law. The truncation causes the transition to normal statistics as $t \to \infty$. The presence of the quasinormal diffusion region for small times is related to the walk in the homogeneous region at the initial stage; the influence of the inhomogeneity is manifested at large scales.

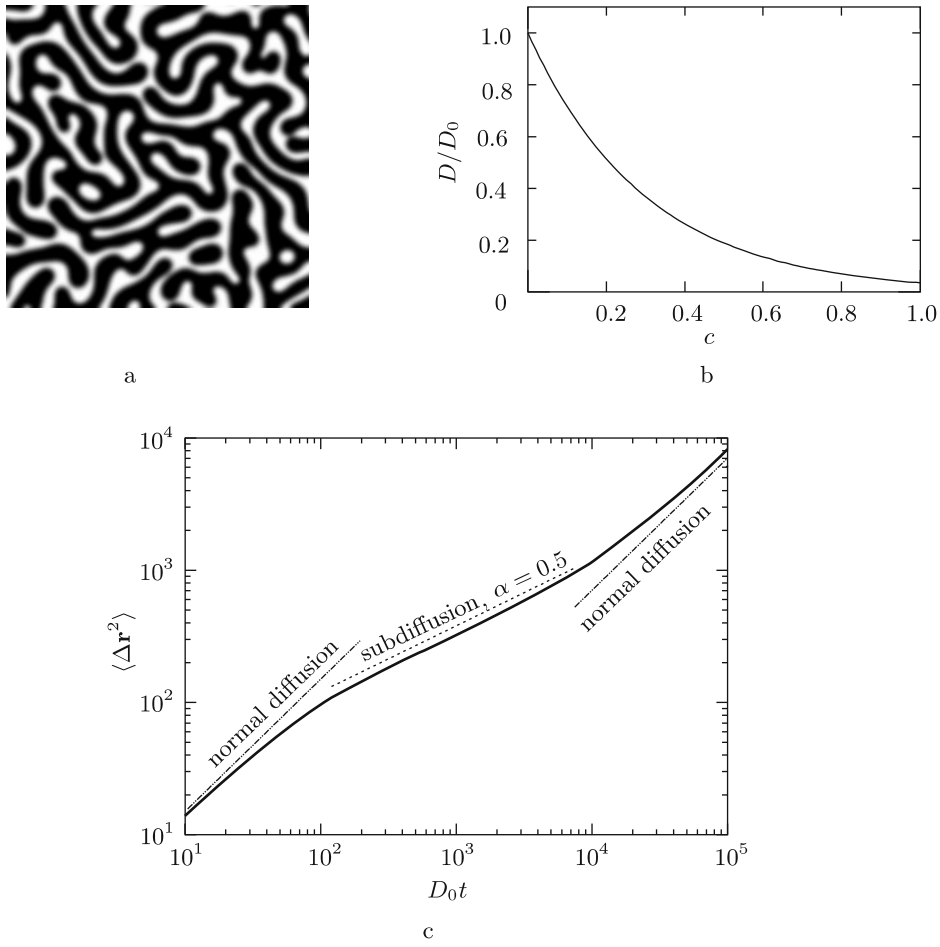

Fig. 1. Realization of anomalous diffusion in the case of a particle walk on the planar realization of the spinodal decomposition of a two-component solution: (a) the pattern of the spinodal decomposition simulated by the Monte Carlo method in the framework of the Cahn–Hilliard approach, (b) the given composition dependence of the diffusion coefficient, and (c) the dependence of the average squared particle displacement during diffusion process obtained by Monte Carlo simulation.

The authors of [37] used a so-called "gradually truncated power law" as a distribution of waiting times. Representing $\Psi(t)$ in the analogous form

$$\Psi(t) \sim \frac{At^{-\alpha}e^{-\beta t}}{\Gamma(1-\alpha)}$$

and using Eq. (7), we obtain the diffusion equation with a truncated fractional derivative:

$$e^{-\beta t}\,{}_0\mathsf{D}_t^{\alpha} e^{\beta t} p(x,t) - C_{\alpha,\beta}\frac{\partial^2}{\partial x^2}p(x,t) = N\delta(x)\frac{t^{-\alpha}e^{-\beta t}}{\Gamma(1-\alpha)}. \tag{13}$$

The generalized Fick law in this case becomes

$$j(x,t) = -C_{\alpha,\beta}\frac{\partial}{\partial t}e^{-\beta t}\,{}_0\mathsf{I}_t^{\alpha} e^{\beta t}\frac{\partial p(x,t)}{\partial x}, \tag{14}$$

where ${}_0\mathsf{I}_t^{\alpha}$ is the Riemann–Liouville fractional integral. Equations (13) and (14) can be used to describe effects related to suppressing the subdiffusion behavior and passing to Gaussian statistics at large times.

3. Subdiffusion generalization of the Ham model

The process of precipitate growth controlled by normal diffusion is considered in the Ham theory of the decomposition of an supersaturated solid solution [2]. Ham primarily considered the boundary-value problem for diffusion equation (8) under the condition that the size of a new-phase precipitate changes very slowly. This is true if the nucleus size is small compared with the size of the cell in which the growth is considered and if the density of new-phase precipitates significantly exceeds that of impurities in the matrix. The boundary conditions formulated for the normal diffusion equation in [2] have the forms

$$\rho(\mathbf{r}(S),t)=\rho_{\mathrm{I}},\qquad \mathbf{n}_T\nabla\rho(\mathbf{r}(T),t)=0.$$

The first condition means that the solution density on the precipitate surface is equal to the equilibrium quantity ρ_{I} with a constant value under given external conditions. It was assumed in [2] that the new-phase precipitate has a spherical shape (S is the spherical cluster surface) and the cluster size is small compared with the distance between the clusters. Nuclei are distributed uniformly over the sample, and the sample can therefore be divided into cells. It can be assumed that new phase precipitates are located at the centers of these cells and the boundaries T are the surfaces of the Wigner–Seitz cells. The second boundary condition therefore suggests that the solution concentrations on both sides of the boundary are approximately the same, and there is no particle flux from one cell to another.

Solving the boundary value problem under the indicated assumptions, Ham showed [2] that at the cluster boundary,

$$\nabla\rho(\mathbf{r},t)|_{r=r_{\mathrm{c}}}\approx\frac{\bar{\rho}(t)}{r_{\mathrm{c}}},\tag{15}$$

where $\bar{\rho}(t)$ is the cell-averaged density of "monomers" (nonprecipitated particles). An analogous consideration of an equivalent boundary value problem, but for fractional differential equation (8), led us to the same expression [38].

Integrating continuity equation (11), where $\mathbf{j}$ is determined in accordance with generalized Fick law (12), over the volume of an equivalent sphere using the Gauss theorem, we obtain the relation

$$\frac{dN}{dt}+\int_S d\mathbf{S}\,C_\alpha\,{}_0\mathsf{D}_t^{1-\alpha}\nabla\rho(\mathbf{r},t)=0.\tag{16}$$

Here, the integral is taken over the cell and cluster surfaces, and the flux through the cell surface is zero (the second boundary condition). Only the integral over the spherical precipitate surface remains. The integration domain varies with time because the clusters grow. In Eq. (16), N is the number of "free" (nonprecipitated) particles in the cell, which is related to the average concentration by the expression

$$N=\bar{\rho}(t)\frac{4}{3}\pi r_{\mathrm{s}}^3.\tag{17}$$

In view of the spherical symmetry, the particle concentration on the surface is uniform. Consequently, taking the surface integral in (16) reduces to multiplying the integrand by the sphere area; using (17), we obtain

$$\frac{4}{3}\pi r_{\mathrm{s}}^3\frac{d\bar{\rho}(t)}{dt}=-4\pi r_{\mathrm{c}}^2C_\alpha\,{}_0\mathsf{D}_t^{1-\alpha}\nabla\rho(\mathbf{r},t).\tag{18}$$

Substituting relation (15) in the right-hand side of Eq. (18), we obtain the equation

$$r_{\mathrm{s}}^3\frac{d\bar{\rho}(t)}{dt}=-3r_{\mathrm{c}}C_\alpha\,{}_0\mathsf{D}_t^{1-\alpha}\bar{\rho}(t).\tag{19}$$

From the conservation law for the total number of particles (also free in the cluster), we have

$$\frac{4\pi}{3}\rho_{\rm c}[r_{\rm c}^3(t) - r_{\rm c}^3(0] = \frac{4\pi}{3}r_{\rm s}^3[\rho_0 - \bar{\rho}(t)]. \tag{20}$$

The left-hand side in this relation is the number of particles added to the cluster during the time t; it is expressed in terms of the variation in the cluster volume. Here, $\rho_{\rm c}$ is the average particle concentration in the cluster. The right-hand side is approximately equal to the same number (we neglect the size of the spherical precipitate) but expressed in terms of the variation in the density of "free" particles in the matrix.

From relation (20), we obtain

$$r_{\rm c}(t) = \left[r_{\rm c}^3(0) + \frac{r_{\rm s}^3}{\rho_{\rm c}}(\rho_0 - \bar{\rho}(t))\right]^{1/3}. \tag{21}$$

We substitute this expression in relation (19) and obtain the fractional differential equation describing the kinetics of new-phase precipitate growth controlled by subdiffusion:

$$\frac{d\bar{\rho}(t)}{dt} = -\frac{3C_\alpha}{r_{\rm s}^3}\left[r_{\rm c}^3(0) + \frac{r_{\rm s}^3}{\rho_{\rm c}}(\rho_0 - \bar{\rho}(t))\right]^{1/3} {}_0{\rm D}_t^{1-\alpha}\bar{\rho}(t). \tag{22}$$

This equation can be solved using one of the specially developed numerical methods for fractional differential equations [39]–[42]. An asymptotic analysis of formula (22) in [38] showed that for rather small t, if we set $\bar{\rho}(t) \approx \rho(0)$, the solution can be represented in the form

$$\bar{\rho}(t) \approx \rho_0 \exp\left\{-\left(\frac{2C_\alpha(\alpha)}{r_{\rm s}^2}\right)^{3/2}\sqrt{\frac{\rho_0}{\rho_{\rm c}}}\,\frac{t^{3\alpha/2}}{[\Gamma(\alpha+1)]^{3/2}}\right\}. \tag{23}$$

This expression is the generalized Ham formula. We note that the diffusion coefficient C_α is also determined by a formula that differs from the classical formula (see [17] for the details). For large t, we have $\bar{\rho}(t) \ll \rho_0$, and from Eq. (22), we find that the solution is expressed in terms of a special function, the Mittag-Leffler function [43]

$$E_\alpha(x) = \sum_{n=0}^{\infty}\frac{x^n}{\Gamma(an+1)}, \quad 0 < \alpha < 1,$$

which plays an important role in the fractional differential calculus [31]. The solution is given by the formula

$$\bar{\rho}(t) = \rho_0 E_\alpha(-Kt^\alpha) \sim \frac{\rho_0}{K}\frac{t^{-\alpha}}{\Gamma(1-\alpha)}, \quad t \gg K^{-1/\alpha}. \tag{24}$$

Here,

$$K = \frac{3C_\alpha}{r_{\rm s}^3}\left[r_{\rm c}^3(0) + \frac{r_{\rm s}^3}{\rho_{\rm c}}\rho_0\right]^{1/3}.$$

The change in the sizes of new-phase precipitates can be calculated using relation (21). For small times, we obtain

$$r_{\rm c}(t) = [r_{\rm c}^3(0) + R^3]^{1/3}, \tag{25}$$

where

$$R = \sqrt{\frac{2C_\alpha(\alpha)}{\Gamma(\alpha+1)}\,\frac{\rho_0}{\rho_{\rm c}}}\,t^{\alpha/2}. \tag{26}$$

For large times, we obtain

$$r_{\rm c}(t) = \left[r_{\rm c}^3(0) + r_{\rm s}^3\frac{\rho_0}{\rho_{\rm c}}\big(1 - E_\alpha(-Kt^\alpha)\big)\right]^{1/3}. \tag{27}$$

Figure 2 shows the comparison of analytic solutions (25) with the numerical solutions for Eqs. (21) and (22) and with the result of the Monte Carlo simulation (see Fig. 2b) described in the next section.

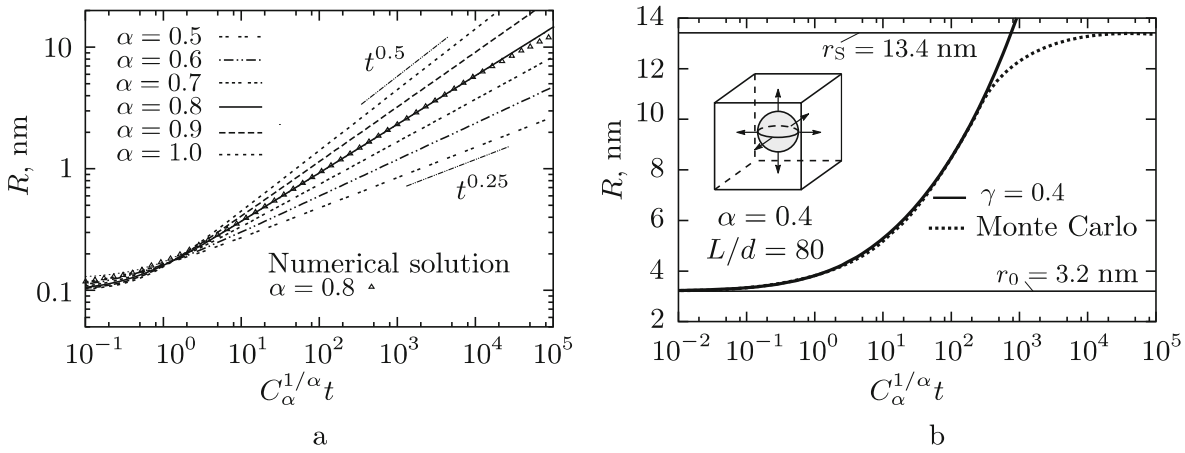

Fig. 2. (a) The time dependence of the precipitate radius for different values of α: the lines correspond to the graphs of function (25), and the points correspond to the solution of (21), where $\bar{\rho}(t)$ was found using the finite-difference numerical scheme for fractional differential equation (22). The chosen parameters are $r_c(0) = 0.1\,\text{nm}$, $r_s = 100\,\text{nm}$, and $\rho_c/\rho_0 = 100$. (b) Solution (25) compared with the result of the Monte Carlo simulation in the case $\alpha = 0.4$.

4. Monte Carlo simulation in the framework of the Ham approach

The Monte Carlo algorithm for solving an integro-differential equation with a fractional derivative proposed in [44] was based on using the model of the fractional Poisson process [45]. This algorithm was used to solve the dispersive transport equation for disordered semiconductors. Here, we use this algorithm to calculate the many-particle problem of the subdiffusion decomposition of solid solutions at the stage of growth of new-phase particles with different shapes. Spherical-precipitate growth was modeled in [38].

The process of the growth of new-phase particles limited by subdiffusion was modeled as follows. An ensemble consisting of N_p particles uniformly distributed in a cubic cell of size L was generated. This cell contained a new-phase nucleus at its center. We assigned each particle coordinates x_i, y_i, and z_i and a time T_i of localization in a trap randomly selected according to the law [45] (here and hereafter, the equality sign $\stackrel{d}{=}$ denotes coincidence between the distributions)

$$T \stackrel{d}{=} \frac{|\log U_1|^{1/\alpha}}{\mu^{1/\alpha}} \frac{\sin(\alpha\pi U_2)[\sin((1-\alpha)\pi U_2)]^{1/\alpha-1}}{[\sin(\pi U_2)]^{1/\alpha}[\log U_3]^{1/\alpha-1}}, \tag{28}$$

where U_1, U_2, and U_3 are independent random numbers uniformly distributed on the interval $(0, 1)$. For $\alpha = 1$, this algorithm reduces to the well-known algorithm for modeling the random quantity $T \stackrel{d}{=} |\log U|/\mu$ with the exponential distribution. The distribution of waiting times (28) is shown in Fig. 3a. For all values $0 < \alpha < 1$, the function $\Psi(t)$ is characterized by the power asymptotic behavior $t^{-\alpha}$ as $t \to \infty$. For $\alpha \to 1$, we have $\Psi(t) \to e^{-\mu t}$.

The set of particles was ranked in accordance with the increase in T_i. Number 1 was assigned to the particle with the smallest waiting time, and so on. Naturally, the particle with the smallest T escapes from the trap before the other particles, i.e., the hop into one of the neighboring free sites is randomly selected for the particle with number 1. If the particle enters the site adjoining the new-phase precipitate, it becomes part of it and leaves the ensemble of "free" particles. The time of particle attachment was fixed. The order of all remaining particles decreases by unity. The cluster radius was recalculated in accordance with its density. Of course, the attachment conditions can be modified. Primarily, we were interested in the

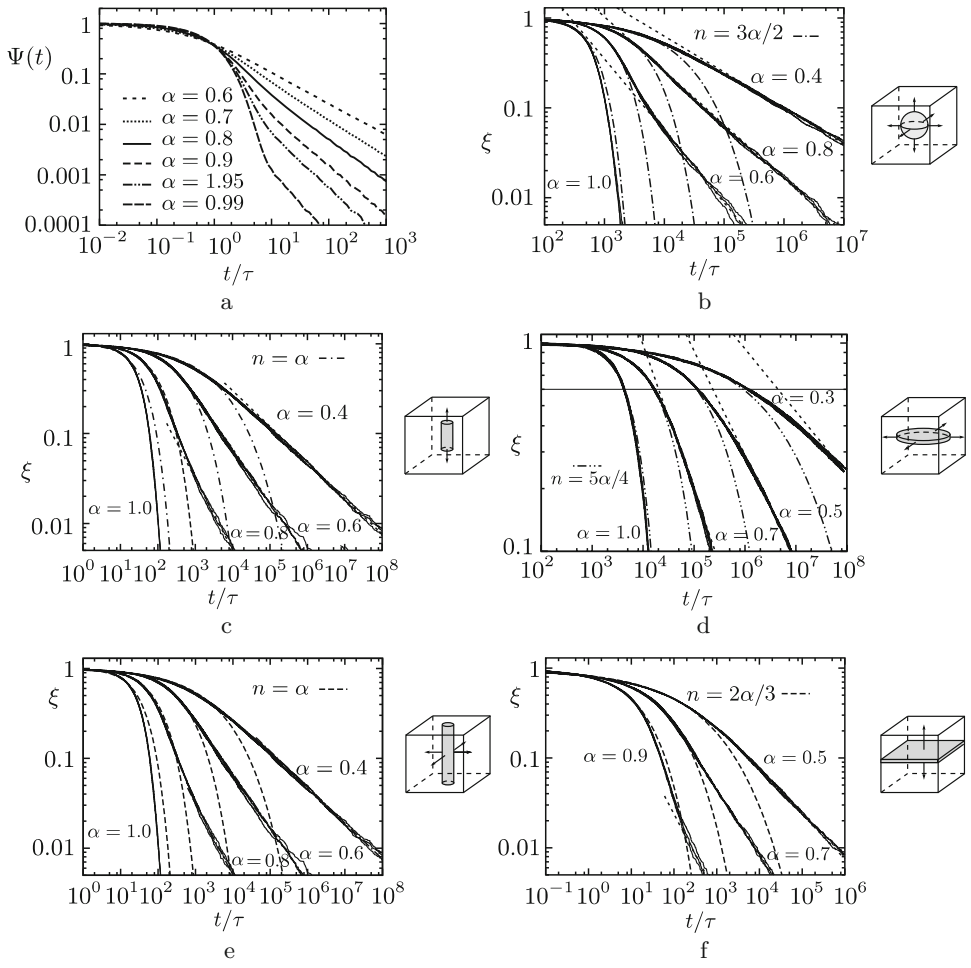

Fig. 3. Results of the Monte Carlo simulation of the kinetics of growth of precipitates with different shapes in the framework of the subdiffusion generalization of the Ham approach: (a) the additional function of the waiting time distribution and (b–f) the time dependence of the decrease in the degree of supersaturation in the case of precipitates with different shapes and growth directions, (b) spherical (isotropic growth), (c) cylindrical (growth in height), (d) disk-shaped (increase in radius), (e) rod-shaped (increase in the radius), and (f) flat precipitates.

influence of subdiffusion on the precipitation kinetics. If the site entered by the particle does not adjoin the new-phase precipitate, then the particle is again localized, and the waiting time ΔT_1 added to the current time T_1 is randomly selected. The particle with the assigned time $T_1 + \Delta T_1$ and new coordinates now occupies the prescribed place k in the ranked particle row after all particles with a number not exceeding k decrease their numbers by unity. The process ends when all particles become parts of the new-phase precipitate.

The important advantage of the algorithm (for example, in comparison with the scheme in which delocalization rates are randomly selected) is that the counting rate is directly independent of the time of new-phase precipitate growth and, consequently, independent of α.

Figure 3b shows the results of the numerical calculations of the kinetics of growth of spherical new-phase precipitates for different values of α. The ratio of the densities is $\rho_c/\rho_0 = 6.4$, and the number of particles is $N_p = 10^4$. The time scale parameter was chosen for each case of α for the curves to be shown in

the same graph. The "tails" of these dependences are compared with the power laws (24), and the initial sections are compared with dependences (23). The results of the numerical calculations thus agree with the analytic solutions. The results for three cell realizations are given for each value of α. Figures 3c–3f show the simulation results for different precipitate shapes and growth directions; the curves were approximated by the dependence $e^{-At^{n\alpha}}$ in the initial stage (the values of n are shown in the figure) and by the dependence $t^{-\alpha}$ in the final stage.

5. Subdiffusion generalization of the Aaron–Kotler model

The Stefan boundary value problem was formulated in [6], [7] to describe the evolution of an isolated spherical precipitate in an infinite matrix: it is necessary to solve the equation of normal isotropic diffusion with the boundary conditions

$$\rho(r,t)|_{r=R} = \rho_{\text{I}}, \qquad \rho(r,t)|_{r\to\infty} = \rho_{\text{M}}, \tag{29}$$

$$(\rho_{\text{p}} - \rho_{\text{I}})\frac{dR}{dt} = D\frac{\partial\rho}{\partial r}\bigg|_{r=R}, \quad t > 0, \tag{30}$$

and the initial condition

$$\rho(r,t)|_{t=0} = \rho_{\text{M}}, \quad r > R. \tag{31}$$

Here, ρ_{p} and ρ_{M} are the respective particle concentrations in the precipitate and the matrix at infinity, and ρ_{I} is the equilibrium concentration on the precipitate surface on the matrix side.

We modify this problem for the case of the subdiffusion-limited decomposition (or dissolution) of the spherical precipitate. We write the equation of isotropic subdiffusion in spherical coordinates:

$$\frac{\partial\rho}{\partial t} = C_\alpha\, {}_0\mathsf{D}_t^{1-\alpha}\left[\frac{\partial^2\rho}{\partial r^2} + \frac{2}{r}\frac{\partial\rho}{\partial r}\right]. \tag{32}$$

Boundary conditions (29) are still applicable in the subdiffusion case, but expression (30) for the boundary motion in accordance with relations (11) and (12) is replaced with the equation

$$(\rho_{\text{p}} - \rho_{\text{I}})\frac{dR}{dt} = C_\alpha\, {}_0\mathsf{D}_t^{1-\alpha}\left[\frac{\partial\rho}{\partial r}\right]_{r=R} \tag{33}$$

or the equation (in the case $\rho_{\text{I}} = \text{const}$)

$$(\rho_{\text{p}} - \rho_{\text{I}})\, {}_0\mathsf{D}_t^{\alpha} R = C_\alpha \frac{\partial\rho}{\partial r}\bigg|_{r=R}. \tag{34}$$

We solve this problem for the fractional differential equation of diffusion in the "stationary interface" approximation assuming slow motion of the precipitate boundary, i.e., satisfaction of the condition $|\rho_{\text{M}} - \rho_{\text{I}}| \ll \rho_{\text{p}} - \rho_{\text{I}}$. In the framework of this approximation, the diffusion equation with the given boundary conditions at the fixed boundary $R = \text{const}$ for an arbitrary R is solved first. Then, after the solution is substituted in Eq. (33), the dependence $R(t)$ is found. Passing to the function $u(r,t) = r[\rho(r,t) - \rho_{\text{M}}]$, we obtain the equation

$$\frac{\partial u}{\partial t} = C_\alpha\, {}_0\mathsf{D}_t^{1-\alpha}\frac{\partial^2 u}{\partial r^2} \tag{35}$$

with the boundary conditions

$$u(r,t)|_{r=R} = R(\rho_{\text{I}} - \rho_{\text{M}}), \qquad u(r,t)|_{r\to\infty} = 0, \quad t > 0, \tag{36}$$

and the initial condition $u(r,t)|_{t=0} = 0$ for $r > R$. If the last condition is taken into account, then relation (35) can be rewritten in the form

$$ {}_0\mathsf{D}_t^{\alpha} u = C_\alpha \frac{\partial^2 u}{\partial r^2}, \tag{37}$$

and its Laplace transformation leads to the equation

$$ s^\alpha \tilde{u}(r,s) - C_\alpha \frac{\partial^2 \tilde{u}(r,s)}{\partial r^2} = 0.$$

With the indicated boundary conditions taken into account, the solution of this equation has the form

$$ \tilde{u}(r,s) = \frac{R(\rho_{\text{I}} - \rho_{\text{M}})}{s} \exp\left\{ -(r-R) \frac{s^{\alpha/2}}{\sqrt{C_\alpha}} \right\}.$$

Passing to the concentration transform, we obtain

$$ \tilde{\rho}(r,s) = \frac{\rho_{\text{M}}}{s} + \frac{\tilde{u}(r,s)}{r} = \frac{\rho_{\text{M}}}{s} + \frac{R(\rho_{\text{I}} - \rho_{\text{M}})}{rs} \exp\left\{ -(r-R) \frac{s^{\alpha/2}}{\sqrt{C_\alpha}} \right\}.$$

The inverse Laplace transformation leads to the expression

$$ \rho(r,t) = \rho_{\text{M}} + \frac{R(\rho_{\text{I}} - \rho_{\text{M}})}{r} \int_0^t d\tau \left(\frac{r-R}{\sqrt{C_\alpha}} \right)^{-2/\alpha} g_+^{(\alpha/2)} \left(\tau \left[\frac{r-R}{\sqrt{C_\alpha}} \right]^{-2/\alpha} \right)$$

or

$$ \rho(r,t) = \rho_{\text{M}} + \frac{R(\rho_{\text{I}} - \rho_{\text{M}})}{r} G_+^{(\alpha/2)} \left(t \left[\frac{r-R}{\sqrt{C_\alpha}} \right]^{-2/\alpha} \right). \tag{38}$$

Here, $g_+^{(\gamma)}(t)$ is the one-sided stable density with the characteristic exponent γ (subordinator), and $G_+^{(\gamma)}(t)$ is the corresponding distribution function [17].

The value of the concentration gradient

$$ \frac{\partial \rho}{\partial r} = - \frac{R(\rho_{\text{I}} - \rho_{\text{M}})}{r^2} G_+^{(\alpha/2)} \left(t \left[\frac{r-R}{\sqrt{C_\alpha}} \right]^{-2/\alpha} \right) -$$

$$ - \frac{2t}{\alpha \sqrt{C_\alpha}} \left(\frac{r-R}{\sqrt{C_\alpha}} \right)^{-2/\alpha - 1} \frac{R(\rho_{\text{I}} - \rho_{\text{M}})}{r} g_+^{(\alpha/2)} \left(t \left[\frac{r-R}{\sqrt{C_\alpha}} \right]^{-2/\alpha} \right)$$

on the precipitate surface $r = R$ (when the asymptotic form of the stable distribution density [17] is used) becomes

$$ \left. \frac{\partial \rho}{\partial r} \right|_{r \to R} = \frac{\rho_{\text{M}} - \rho_{\text{I}}}{R} + \frac{t^{-\alpha/2} (\rho_{\text{M}} - \rho_{\text{I}})}{\Gamma(1 - \alpha/2) \sqrt{C_\alpha}}.$$

Substituting the last relation in Eq. (34) for the function $R(t)$ leads to the equation

$$ {}_0\mathsf{D}_t^{\alpha} R = C_\alpha \frac{\beta(R)}{R} + \sqrt{C_\alpha} \frac{\beta(R) t^{-\alpha/2}}{\Gamma(1 - \alpha/2)}, \qquad \beta(R) = \frac{\rho_{\text{M}} - \rho_{\text{I}}(R)}{\rho_{\text{p}} - \rho_{\text{I}}(R)}. \tag{39}$$

In the case where $\alpha = 1$ and $C_1 = D$, we have

$$ \rho(r,t) = \rho_{\text{M}} + \frac{R(\rho_{\text{I}} - \rho_{\text{M}})}{r} G_+^{(1/2)} \left(t \left[\frac{r-R}{\sqrt{D}} \right]^{-2} \right) = \rho_{\text{M}} + \frac{R(\rho_{\text{I}} - \rho_{\text{M}})}{r} \operatorname{erfc} \left(\frac{r-R}{2\sqrt{Dt}} \right),$$

i.e., we obtain the classical result, which is applicable for normal diffusion [6].

We consider the case where the growth of the spherical new-phase precipitate is controlled by subdiffusion under the condition $\rho_{\mathrm{I}}(R) = \text{const}$ and accordingly $\beta = (\rho_{\mathrm{M}} - \rho_{\mathrm{I}})/(\rho_{\mathrm{p}} - \rho_{\mathrm{I}}) = \text{const}$. We seek the solution of Eq. (39) in the form

$$R(t) = \lambda(C_\alpha t^\alpha)^{1/2}. \tag{40}$$

Substituting this function and the fractional derivative of it

$$
\begin{aligned}
{}_0\mathsf{D}_t^\alpha R &= \frac{\lambda C_\alpha^{1/2}}{\Gamma(1-\alpha)}\frac{d}{dt}\int_0^t d\tau\,\tau^{\alpha/2}(t-\tau)^\alpha = \frac{(1-\alpha/2)\lambda C_\alpha^{1/2}}{\Gamma(1-\alpha)}t^{-\alpha/2}\mathrm{B}\left(1+\frac{\alpha}{2};1-\alpha\right) = \\
&= \frac{\alpha\Gamma(\alpha/2)}{\Gamma(1-\alpha/2)}\lambda C_\alpha^{1/2}t^{-\alpha/2}
\end{aligned}
$$

in formula (39) leads to the quadratic equation

$$\alpha\Gamma\left(\frac{\alpha}{2}\right)\lambda^2 - \beta\lambda - \Gamma\left(1-\frac{\alpha}{2}\right)\beta = 0,$$

which has the positive root

$$\lambda = \frac{\beta + \sqrt{\beta^2 + 4\beta\pi\alpha/\sin\pi\alpha}}{2\alpha\Gamma(\alpha/2)}. \tag{41}$$

Hence, expression (40) gives the law of subdiffusion-limited growth of a spherical precipitate for constant β and generalizes the expression $R(t) \propto t^{1/2}$ obtained for normal diffusion [6].

For spherical precipitates, the equilibrium concentration ρ_{I} of particles near the precipitate surface on the side of the matrix is given by the Gibbs–Thomson expression

$$\rho_{\mathrm{I}} = \rho_{\mathrm{I}}^\infty \exp\left(\frac{A}{kTR}\right), \tag{42}$$

where A is a composition-dependent constant. For Cu in α-Fe, $A = 672.51\,k$ [46].

Figure 4 shows the results of the Monte Carlo simulation of the spherical precipitate dissolution for normal impurity diffusion with the Gibbs–Thomson effect taken into account. Equation (39) for the function $R(t)$ can also be solved using one of the numerical methods that were especially developed for fractional-order differential equations [39]–[42].

The results of the solution using the finite-difference method (after the approximation of the Riemann–Liouville fractional derivative by the Grünwald–Letnikov derivative) are shown in Fig. 5. The kinetics of dissolution and growth of spherical precipitates with decreasing α decreases (becomes more gently sloping). In the case of growth, the curves in the large-time limit tend to the dependence $t^{\alpha/2}$. In the limit $\alpha \to 1$, the solutions found using the special numerical algorithm for fractional values of α approach the result calculated by the standard finite-difference method in the case $\alpha = 1$, which is in turn close to the curve found using the Monte Carlo simulation. This indicates satisfaction of the correspondence principle and the applicability of the stationary interface approximation for the chosen parameters.

6. Conclusions

We have considered the kinetics of subdiffusion-limited growth and dissolution of new-phase particles in solid solutions using an up-to-date approach based on kinetic equations with fractional-order derivatives and the corresponding algorithms for the Monte Carlo simulation. We considered generalizations of the well-known Ham [2], [3] and Aaron–Kotler [6], [7] precipitation models. The solutions obtained in the framework

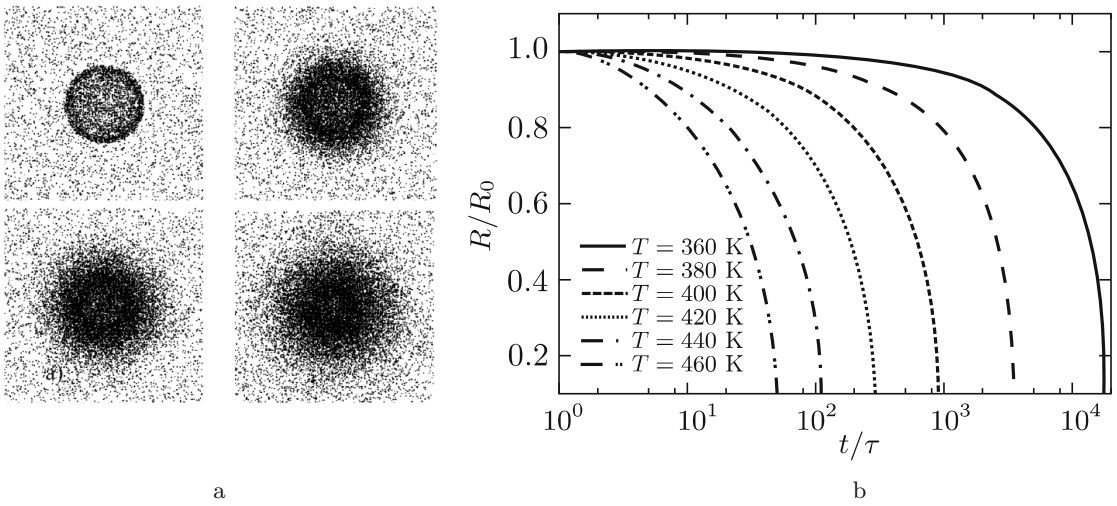

Fig. 4. Results of the Monte Carlo simulation of spherical precipitate dissolution for normal impurity diffusion with the Gibbs–Thomson effect taken into account: (a) evolution of the impurity distribution near the precipitate projected on the xy plane and (b) the kinetics of diffusion-limited dissolution at different temperatures.

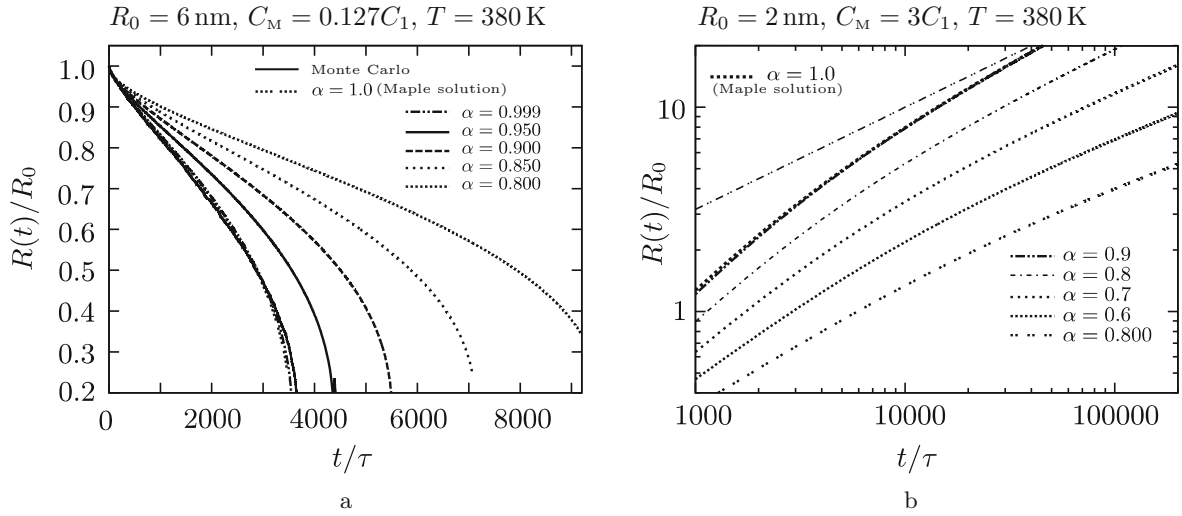

Fig. 5. Kinetics of subdiffusion (a) dissolution and (b) growth of spherical precipitates for different anomalous-diffusion exponents α calculated in the framework of the fractional differential generalization of the Aaron–Kotler model.

of these generalizations agree with the results of the Monte Carlo simulation. Using the simulation, we considered the kinetics of growth of precipitates with different shapes: spherical, disk-shaped, cylindrical, and rod-shaped ones and some others. As the precipitates grow, the initial section of the supersaturation decrease curve is described by the dependence $\sim e^{-kt^{n\alpha}}$, and the large-time asymptotic behavior is of the power-law type with the exponent $-\alpha$ for all considered shapes. In the generalized Aaron–Kotler model, the analytic results were mainly obtained in the stationary interface approximation. The particle profiles in the matrix were expressed in terms of stable distributions that are a generalization of the Gaussian distribution. If the Gibbs–Thomson effect is not taken into account, then we found that in the subdiffusion generalizations of the Ham and Aaron–Kotler models, the kinetics of the spherical cluster growth is described by the power

law $\propto t^{\alpha/2}$. If the Gibbs–Thomson effect is taken into account, then the time dependence of the radius turns out to be steeper in the initial growth stages and becomes the power-law dependence $t^{\alpha/2}$ in the large-time limit.

The obtained results can turn out to be useful for analyzing experimental and model data on precipitation. In particular, the existing data for the Cu–Fe system [47]–[51] are evidence of the power-law growth of spherical Cu precipitates in α-Fe with the exponent 0.4, which contradicts the results of the mentioned normal-diffusion models and the classical coalescence model. The data in [52] on Si nanoprecipitate dissolution in an Al matrix at annealing temperatures of 500–560 °C showed behavior that is slower than is predicted by the classical diffusion model of spherical precipitate dissolution [53]. In connection with this, we plan to devote the next paper to a detailed analysis of existing experimental data in the framework of the presented fractional differential models.

Acknowledgments. This work was supported by the Russian Foundation for Basic Research (Grant No. 15-01-99674) and the Russian Federation Ministry of Education and Science in the framework of state task 2014/296 (1643, 3.1862.2014K).

REFERENCES

1. V. V. Slezov and V. V. Sagalovich, *Sov. Phys. Usp.*, **30**, 23–45 (1987).
2. F. S. Ham, *J. Phys. Chem. Solids*, **6**, 335–351 (1958).
3. F. S. Ham, *J. Appl. Phys.*, **30**, 1518–1525 (1959).
4. H. B. Aaron, *Metal Sci.*, **2**, 192–193 (1968).
5. M. J. Whelan, *Metal Sci.*, **3**, 95–97 (1969).
6. H. B. Aaron, D. Fainstein, and G. R. Kotler, *J. Appl. Phys.*, **41**, 4404–4410 (1970).
7. H. B. Aaron and G. R. Kotler, *Metal. Mater. Trans. B*, No. 2, 393–408 (1971).
8. A. V. Gapontsev and V. V. Kondrat'ev, *Phys. Usp.*, **46**, 1077–1098 (2003).
9. V. L. Gapontsev, I. K. Rasumov, Yu. N. Gornostyrev, A. E. Ermakov, and V. V. Kondrat'ev, *Phys. Metals Metallogr.*, **99**, 365–375 (2005).
10. I. M. Lifshits and V. V. Slezov, *Sov. Phys. JETP*, **8**, 331–339 (1959).
11. S. Liu, L. Bönig, J. Detch, and H. Metiu, *Phys. Rev. Lett.*, **74**, 4495–4498 (1995).
12. J. P. Bouchaud and A. Georges, *Phys. Rep.*, **195**, 127–293 (1990).
13. M. B. Isichenko, *Rev. Modern Phys.*, **64**, 961–1043 (1992).
14. R. Metzler and J. Klafter, *Phys. Rep.*, **339**, 1–77 (2000).
15. Y. Gefen, A. Aharony, and S. Alexander, *Phys. Rev. Lett.*, **50**, 77–80 (1983).
16. S. B. Yuste and K. Lindenberg, *Chem. Phys.*, **284**, 169–180 (2002).
17. V. V. Uchaikin, *Phys. Usp.*, **46**, 821–849 (2003).
18. V. V. Uchaikin and R. T. Sibatov, *Fractional Kinetics in Solids: Anomalous Charge Transport in Semiconductors, Dielectrics, and Nanosystems*, CRC Press, Boca Raton, Fla. (2013).
19. R. T. Sibatov and V. V. Uchaikin, *Phys. Usp.*, **52**, 1019–1043 (2009).
20. R. T. Sibatov and V. V. Uchaikin, *Semiconductors*, **41**, 335–340 (2007).
21. V. V. Uchaikin and R. T. Sibatov, *JETP Letters*, **86**, 512–516 (2007).
22. V. P. Shkilev, *JETP*, **116**, 703–710.
23. P. Paradisi, R. Cesari, F. Mainardi, and F. Tampieri, *Phys. A*, **293**, 130–142 (2001).
24. V. M. Kenkre, E. W. Montroll, and M. F. Shlesinger, *J. Statist. Phys.*, **9**, 45–50 (1973).
25. M. F. Shlesinger, *J. Statist. Phys.*, **10**, 421–434 (1974).
26. H. Scher and E. W. Montroll, *Phys. Rev. B*, **12**, 2455–2477 (1975).
27. J. Klafter and R. Silbey, *Phys. Rev. Lett.*, **44**, 55–58 (1980).
28. A. Blumen, J. Klafter, and G. Zumofen, *Phys. Rev. B*, **27**, 3429–3435 (1983).
29. R. Gorenflo, F. Mainardi, and A. Vivoli, *Chaos Solitons Fractals*, **34**, 87–103 (2007); arXiv:cond-mat/0701126v3 (2007).

30. E. W. Montroll and G. H. Weiss, *J. Math. Phys.*, **6**, 167–181 (1965).
31. V. V. Uchaikin, *Method of Fractional Derivatives* [in Russian], Artishok, Ulyanovsk (2008).
32. K. B. Oldham and J. Spanier, *The Fractional Calculus* (Math. Sci. Engin., Vol. 111), Acad. Press, New York (1974).
33. I. Podlubny, *Fractional Differential Equations* (Math. Sci. Engin., Vol. 198), Acad. Press, San Diego, Calif. (1999).
34. J. W. Cahn and J. E. Hilliard, *J. Chem. Phys.*, **28**, 258–267 (1958).
35. A. Milchev, D. W. Heermann, and K. Binder, *Acta Metallurgica*, **36**, 377–383 (1988).
36. E. Sander and T. Wanner, *J. Statist. Phys.*, **95**, 925–948 (1999).
37. A. Cortis, C. Gallo, H. Scher, and B. Berkowitz, *Water Resour. Res.*, **40**, W04209 (2004).
38. V. V. Svetukhin and R. T. Sibatov, *JETP*, **120**, No. 4, 678–686 (2015).
39. K. Diethelm and N. J. Ford, *J. Math. Anal. Appl.*, **265**, 229–248 (2002).
40. K. Diethelm, N. J. Ford, and A. D. Freed, *Numer. Algor.*, **36**, 31–52 (2004).
41. K. Diethelm, N. J. Ford, A. D. Freed, and Yu. Luchko, *Comput. Methods Appl. Mech. Engrg.*, **194**, 743–773 (2005).
42. C. Li and F. Zeng, *Numer. Funct. Anal. Optim.*, **34**, 149–179 (2013).
43. F. Mainardi and R. Gorenflo, *J. Comput. Appl. Math.*, **118**, 283–299 (2000).
44. V. V. Uchaikin and R. T. Sibatov, *Russ. J. Numer. Anal. Math. Model.*, **23**, 283–297 (2008).
45. V. V. Uchaikin, D. O. Cahoy, and R. T. Sibatov, *Internat. J. Bifurcation Chaos Appl. Sci. Engrg.*, **18**, 2717–2725 (2008).
46. G. Salje and M. Feller-Kniepmeier, *J. Appl. Phys.*, **48**, 1833–1839 (1977).
47. R. Kampmann and R. Wagner, "Phase transformations in Fe-Cu-Alloys-SANS-experiments and theory," in: *Atomic Transport and Defects in Metals by Neutron Scattering* (Springer Proc. Phys., Vol. 10, C. Janot, W. Petry, and D. Richter, eds.), Springer, New York (1986), pp. 73–77.
48. M. H. Mathon, A. Barbu, F. Dunstetter, F. Maury, N. Lorenzelli, and C. H. De Novion, *J. Nucl. Mater.*, **245**, 224–237 (1997).
49. S. R. Goodman, S. S. Brenner, and J. R. Low, *Metallurgical Transactions*, **4**, 2371–2378 (1973).
50. M. Perez, F. Perrard, V. Massardier, X. Kleber, A. Deschamps, H. De Monestrol, P. Pareige, and G. Covarel, *Philosophical Magazine*, **85**, 2197–2210 (2005).
51. F. Soisson and C.-C. Fu, *Phys. Rev. B*, **76**, 214102 (2007).
52. U. H. Tundal and N. Ryum, *Metal. Trans. A*, **23**, 445–449 (1992).
53. T. L. Durbin, "Modeling dissolution in aluminum alloys," Doctoral dissertation, Mechanical Engineering, Georgia Institute of Technology, Atlanta, Ga. (2005).